Product energy deposition of CN + alkane H abstraction reactions in gas and solution phases

David R. Glowacki, Andrew J. Orr-Ewing, and Jeremy N. Harvey

Citation: J. Chem. Phys. **134**, 214508 (2011); doi: 10.1063/1.3595259
View online: http://dx.doi.org/10.1063/1.3595259
View Table of Contents: http://aip.scitation.org/toc/jcp/134/21
Published by the American Institute of Physics

Product energy deposition of CN + alkane H abstraction reactions in gas and solution phases

David R. Glowacki,[a] Andrew J. Orr-Ewing, and Jeremy N. Harvey
School of Chemistry, University of Bristol, Bristol BS8 1TS, United Kingdom

(Received 14 March 2011; accepted 6 May 2011; published online 7 June 2011)

In this work, we report the first theoretical studies of post-transition state dynamics for reaction of CN with polyatomic organic species. Using electronic structure theory, a newly developed analytic reactive PES, a recently implemented rare-event acceleration algorithm, and a normal mode projection scheme, we carried out and analyzed quasi-classical and classical non-equilibrium molecular dynamics simulations of the reactions CN + propane (R1) and CN + cyclohexane (R2). For (R2), we carried out simulations in both the gas phase and in a CH_2Cl_2 solvent. Analysis of the results suggests that the solvent perturbations to the (R2) reactive free energy surface are small, leading to product energy partitioning in the solvent that is similar to the gas phase. The distribution of molecular geometries at the respective gas and solution phase variational association transition states is very similar, leading to nascent HCN which is vibrationally excited in both its CH stretching and HCN bending coordinates. This study highlights the fact that *significant* non-equilibrium energy distributions may follow in the wake of solution phase bimolecular reactions, and may persist for hundreds of picoseconds despite frictional damping. Consideration of non-thermal distributions is often neglected in descriptions of condensed-phase reactivity; the extent to which the present intriguing observations are widespread remains an interesting question. © *2011 American Institute of Physics*. [doi:10.1063/1.3595259]

I. INTRODUCTION

Our fundamental understanding of chemical dynamics, kinetics, reactivity, and energy transfer in the gas phase has advanced considerably in the past few decades, and increasing efforts are underway to obtain similarly detailed insight into solution phase processes.[1–3] Solution phase chemical reactions are subject to a number of complications compared to their gas phase counterparts – including modifications of reactive potential energy surfaces by the solvent, solvent caging,[4] and solvent friction,[5] all of which combine to affect reaction rates,[6,7] energy transfer,[2] and chemical dynamics.

The microscopic dynamics of a successful bimolecular reaction in solution may be heuristically broken into three consecutive stages. The first stage is that during which the reactants navigate their individual solvent cages, leading to some form of association complex. The second stage includes the time window during which the chemical reaction may be defined as having occurred: following their encounter, there will be some ensemble averaged probability that the reactants' energy and orientation is favorable enough to undergo passage over the potential energy surface saddle point or transitions state (TS), or some other similarly defined point of no return. Averaged over a Boltzmann ensemble, the properties of the first two stages combine to define the phenomenological kinetic rate coefficient for reaction. The third stage of reaction is the so-called post-transition state dynamics stage, during which the reactants relax to equilibrium following TS passage.

In the gas phase, a range of experimental and theoretical studies have demonstrated the prevalence of non-equilibrium (alternatively referred to as non-Markovian, or non-statistical) post-TS dynamics.[8,9] While such post-TS dynamics are interesting *per se* in continued attempts to unravel the fundamental microscopic details of condensed phase chemical reactivity, it may be the case that their effects are even more far ranging than has generally been appreciated. For example, recent work suggests that non-equilibrium post-TS microphysics of solution phase bimolecular reactions may determine product ratios in reactions as ubiquitous as alkene hydroboration,[9,10] which is a staple reaction in synthetic organic chemistry.

Numerous studies have been carried out to determine kinetic rate coefficients for bimolecular reactions in solution. Also, several experimental and theoretical investigations have looked at the microscopic details of energy transfer and dynamics for unimolecular processes following photoexcitation.[7,11–13] However, there have been far fewer experimental and theoretical investigations of the post-transition state dynamics of thermal bimolecular reactions in solution, due to experimental and theoretical difficulties. On the experimental side, such investigations require very fast analytical methods that are capable of resolving solute features from solvent features. On the modeling side, computationally tractable yet accurate reactive potential energy surfaces (PESs) are required for the whole solute-solvent system, as well as methods for accurately addressing the rare event nature of bimolecular encounters in solution.

In this article, we present a molecular modelling study of the post-transition state dynamics for CN + alkane H atom abstraction reactions in both the gas phase and a CH_2Cl_2

[a]Electronic mail: david.r.glowacki@bristol.ac.uk.

(dichloromethane) solvent, initiating our dynamics in the later phases of stage one (described above). The present study was carried out alongside recent time-resolved infrared (IR) post-TS measurements of nascent HCN for the reaction of CN + cyclohexane in solution, in which significant HCN vibrational excitation was observed.[14] This finding differs somewhat from previous studies on the CN + $CHCl_3$ reaction by Hochstrasser and co-workers[15] and by Crim and co-workers,[16] who deduced that the nascent HCN is essentially thermal – leading to the conclusion that the solution phase reaction shows markedly different post-transition state dynamics than in the gas phase. Hochstrasser and Voth attributed this to solvent modifications of the PES, noting that the transition state region in the solution is shifted closer to the HCN product than in the gas phase.[1]

To the best of our knowledge, the work described in this article presents the first molecular dynamics study of abstraction mechanisms for reactions of CN + polyatomic organic molecules. In what follows, we investigated the following reactions

$$CN + C_3H_8 \rightarrow HCN + C_3H_7. \quad \text{(R1)}$$

$$CN + c\text{-}C_6H_{12} \rightarrow HCN + c\text{-}C_6H_{11}. \quad \text{(R2)}$$

(R1) was investigated using gas phase *ab initio* quasiclassical direct dynamics. To investigate (R2), we used an analytic PES which we developed by fitting molecular mechanics force fields to coupled cluster (CCSD(T)) electronic structure theory energies. Subsequently, we carried out both gas and solution phase classical MD simulations using a recently developed MD rare-event acceleration algorithm.[17] In all the simulations, we obtained normal mode energies from the (R1) and (R2) Cartesian dynamics by transforming to the normal mode frame. The MD simulations have afforded a level of detail which was inaccessible in the accompanying experiments, and show that: (1) that the degree of vibrational excitation at short time of both the C–H stretch and the bend in HCN is largely identical in the gas phase and in solution, (2) within the post-TS region, the solution and gas phase reaction free energy profiles are very similar, consistent with the fact that the observed post-TS dynamics at short times are very similar, and (3) in solution phase, the energy relaxation of the nascent excited HCN shows multiple timescales compared to the relaxation of HCN in pure solvent.

II. METHODS

A. *Ab initio* PES: Wave function and DFT approaches

In order to carry out *ab initio* direct dynamics to investigate energy disposal in HCN following CN hydrogen abstraction reactions, the first part of this study involved obtaining an accurate representation of an abstraction PES for reaction of CN with a small alkane. Given the computational expense of obtaining an accurate (R2) PES using high level electronic structure theory, we examined CN abstraction of a secondary H on propane (R1) as a reasonable proxy. An accurate representation of the (R1) potential energy surface (PES) is complicated because the CN radical is poorly described by typical spin-unrestricted methods, which produce significant spin contamination in this system, with consequently unreliable geometries and energies. Restricted open shell treatments produced more reliable energies and geometries, and we obtained an accurate representation of the energetics along the addition PES as follows: (1) Using unrestricted coupled cluster theory on a restricted open shell reference wave function (UCCSD-ROHF) in conjunction with the cc-pVDZ basis set, geometries along the reaction coordinate were obtained by performing relaxed scans along the secondary H–CN approach coordinate; and (2) single point energies along the reaction coordinate were obtained by carrying out further UCCSD(T)-ROHF calculations and extrapolating to the infinite basis set limit using the cc-pVDZ and cc-pVTZ basis sets. The extrapolation formula that we used to determine the infinite basis energy, E_∞, is as follows:[18]

$$E_\infty = E_\ell - \frac{B}{(\ell+1)^4}, \quad (1)$$

where E_ℓ is the CCSD(T) energy obtained using a basis set with a maximum angular momentum basis function ℓ.

Calculating the potential energy and gradient "on the fly" during a classical trajectory study using the UCCSD(T) methods discussed above is computationally unaffordable. Our strategy was instead to use density functional theory (DFT), using a functional selected to reproduce fairly closely the more accurate CCSD(T) PES profile. In conjunction with the 6-31G* basis set, we examined several different functionals including PBE, B1LYP, B3LYP, BB1K, and modified forms of BB1K. We also investigated the use of empirical dispersion corrections, but found that they had little effect. A restricted open shell treatment using the BB1K functional, modified to have 56% exact Hartree-Fock exchange, gave the best agreement with the CCSD(T) relative energies along the (R1) reaction path. All wavefunction based calculations in this work were carried out using the MOLPRO suite of programs, and all DFT calculations were carried out using the GAUSSIAN 03 suite of programs.[19]

B. Gas phase direct dynamics

With the aforementioned modified BB1K functional and the 6-31G* basis set, we carried out quasiclassical direct dynamics calculations using a version of the VENUS dynamics package[20] which we have locally modified to interface with arbitrary electronic structure theory packages. Initial selection of zero point energy corrected coordinates and momenta for CN and propane was performed using microcanonical normal mode sampling,[21] where the normal mode quantum numbers were selected from a 298 K vibrational Boltzmann distribution. Rotational and relative translational energies of each fragment were selected from 298 K Boltzmann distributions, with the orientation of each molecule randomly selected by rotation in the molecular center of mass (COM) Eckart frame. As there is no enthalpic barrier to reaction, there was no need to include additional kinetic energy along the association reaction coordinate in order to observe reactive events. Trajectories were initialized with a 4.5 Å center-of-mass separation between CN and propane fragments. In order to reduce the

computational expense of these calculations, and given that our primary interest in this work is the post-transition state dynamics following H atom abstraction, we: (1) set the impact parameter to zero, and (2) used importance sampling to increase the probability of selecting reactive trajectories, i.e., we only propagated those trajectories which had an initial H–CN separation of less than 4.0 Å. Trajectories which satisfied the importance sampling criteria were propagated 3000 steps using a velocity Verlet integrator and a timestep of 0.2 fs. We monitored total energy conservation for all reactive trajectories and discarded those which did not have a total energy conservation of better than 2.5% with respect to the difference between the initial total energy of CN + C_3H_8, and the final HCN + C_3H_7 potential energy.

C. CN + cyclohexane PES

Running a large number of solution phase trajectories using the DFT direct dynamics techniques described above is computationally expensive, and furthermore, the energetics are not as accurate compared to the CCSD(T) results as we would prefer. Consequently, we also used an analytical form of the PES which we fitted to the electronic theory data described above. The use of matrix representations to construct reactive PESs has been investigated by a number of previous workers, going back to Evans and Polyani,[22] and our strategy is along those same lines. We constructed a reactive PES from a matrix representation of analytical molecular mechanics forcefields, $V(\mathbf{q})$, which are generally well-calibrated for simulations of non-reactive dynamics. The coordinate-dependent Hamiltonian, $\mathbf{H}(\mathbf{q})$, was represented using a symmetric $n \times n$ matrix, where the diagonal elements, $V_i(\mathbf{q})$, are the molecular mechanics energies for a particular connectivity arrangement, and ε_i are corresponding energy offsets associated with reaction endo- or exo-thermicity. The overall potential energy of the system for a given set of nuclear coordinates is then taken as the lowest eigenvalue, $\lambda_0(\mathbf{q})$, of $\mathbf{H}(\mathbf{q})$. In general, the system may be described by an n-state Hamiltonian of the form

$$\mathbf{H}(\mathbf{q}) = \begin{bmatrix} V_1(\mathbf{q}) + \varepsilon_1 & . & . & . & H_{1n}(\mathbf{q}) \\ . & . & & & . \\ . & & . & & . \\ . & & & . & . \\ H_{n1}(\mathbf{q}) & . & . & . & V_n(\mathbf{q}) + \varepsilon_n \end{bmatrix}, \quad (2)$$

in which the off-diagonal elements are identical, i.e., $H_{ij}(\mathbf{q}) = H_{ji}(\mathbf{q})$.

The simplest useful form of Eq. (2) is when $n = 2$, giving a two-state, 2×2 Hamiltonian in which state 1 corresponds to the reactant connectivity, state 2 corresponds to the product connectivity, and there is a single coupling element. In this case, the values of ε_i are generally chosen so that the energies at the respective product and reactant geometries (P and R) give the correct energy of reaction, which is evaluated as $\lambda_0(\mathbf{q} = \mathrm{P}) - \lambda_0(\mathbf{q} = \mathrm{R})$. In the case that the coupling elements, $H_{12}(\mathbf{q} = \mathrm{P})$ and $H_{12}(\mathbf{q} = \mathrm{R})$, are much smaller than the energy gap between the diagonal elements near the product and reactant geometries, then the reaction energy is $(V_2(\mathbf{q} = \mathrm{P}) + \varepsilon_2) - (V_1(\mathbf{q} = \mathrm{R}) + \varepsilon_1)$.

In addition to the total system potential energy obtained via diagonalization of Eq. (2), molecular dynamics approaches also require evaluation of energy gradients. While it is straightforward to write down an analytic expression for $d\lambda_0(\mathbf{q})/d\mathbf{q}$ in the case of a two-dimensional Hamiltonian matrix, this approach is not feasible for the more general case of an n-dimensional Hamiltonian. The diagonal eigenvalue matrix, $\mathbf{D}$, may be written as

$$\mathbf{D} = \mathbf{U}^{\mathrm{T}}\mathbf{H}\mathbf{U}, \quad (3)$$

where $\mathbf{U}$ is the eigenvector matrix, and the elements of $\mathbf{D}$, $\mathbf{U}$, and $\mathbf{H}$ all implicitly depend on $\mathbf{q}$, i.e., they may be written as $\mathbf{D}(\mathbf{q})$, $\mathbf{U}(\mathbf{q})$, and $\mathbf{H}(\mathbf{q})$. The derivatives of the eigenvalues may then be calculated as

$$\frac{d\mathbf{D}}{d\mathbf{q}} = \mathbf{U}^{\mathrm{T}}\frac{d\mathbf{H}}{d\mathbf{q}}\mathbf{U}. \quad (4)$$

This is analogous to the Hellman-Feynmann approach, commonly written as

$$\frac{dE}{d\mathbf{q}} = \langle\psi(\mathbf{q})|\frac{d\mathbf{H}}{d\mathbf{q}}|\psi(\mathbf{q})\rangle, \quad (5)$$

where E and ψ are the lowest eigenvalue and corresponding eigenfunction obtained from solution of the time independent Schrodinger equation. Equations (4) and (5) are accurate so long as the elements of $\mathbf{H}(\mathbf{q})$ are continuously differentiable in the neighborhood of $\mathbf{q}$.[23]

One significant difficulty in a matrix representation of a reactive forcefield such as that in Eq. (2) lies in representing the off-diagonal coupling elements, $H_{ij}(\mathbf{q})$, and a number of different strategies for doing this have been proposed, e.g., the empirical valence bond (EVB) approach of Warshel and Weiss,[24] the approach of Chang and Miller,[25] and Truhlar's multiconfigurational molecular mechanics (MCMM).[26] Because the system under investigation herein involves significant non-equilibrium dynamics, a reasonably accurate representation of the energetics along the reaction path is as important as the energies of the reactant and product states. The approach that we have taken in this work is similar in philosophy to the recently described distributed Gaussian approach,[27] wherein the off-diagonal coupling elements of $\mathbf{H}(\mathbf{q})$ are fit to gas-phase electronic structure theory results for some dynamically significant subset of $\mathbf{q}$. We represented the off diagonal coupling elements as Gaussian functions of the H–CN bond distance, r, i.e.,

$$H_{ij}(r) = A_{ij}\exp\left(-\frac{1}{2}((r_{\mathrm{H-CN}} - B_{ij})/C_{ij})^2\right), \quad (6)$$

where A_{ij}, B_{ij}, and C_{ij} are the respective amplitude, center, and width parameters for off-diagonal coupling element ij.

In the interest of computational efficiency and to avoid over-fitting, it is desirable to minimize the number of coupling elements. In this work, we were able to accurately model the CCSD(T) reaction path between CN and a single cyclohexane hydrogen using a 3×3 Hamiltonian matrix that included a C_6H_{11} + HCN product state (state 1), two degenerate C_6H_{12} + CN reactant states (states 2 and 3), and two non-zero Gaussian coupling elements (H_{12} and H_{13}). This left a total of six Gaussian parameters which we fit to gas phase relaxed scans

along the H–CN coordinate using a Levenberg-Marquardt nonlinear least squares optimization algorithm with numerical gradients. The goodness of fit was determined from a simple merit function

$$\chi^2(A_i, B_i, C_i; i \in k) = \sum_{r \in \text{path}} \left[\frac{\lambda_0(\mathbf{q} = r) - (\Delta E_{\text{CCSD(T)/CBS}}(r))}{\Delta E_{\text{CCSD(T)/CBS}}(r)} \right]^2, \quad (7)$$

where $\Delta E_{\text{CCSD(T)/CBS}}(r) = E_{\text{CCSD(T)/CBS}}(r) - E_{\text{CCSD(T)/}CBS(\infty)}$, i.e., with respect to the reaction asymptote at ∞. Equation (7) was found to satisfactorily weight both the low and high energies along the reaction path. For each trial set of parameters defining the $H_{ij}(\mathbf{q} = r)$ coupling elements, values of $\lambda_0(\mathbf{q} = r)$ were obtained through geometry optimization with the H–CN coordinate, r, constrained to be identical to the corresponding value of r along the CCSD(T) reaction path. Hence the structures are not necessarily identical to those used in the CCSD(T) scans. However, inspection of both sets of structures along the reaction path shows that they are very similar, providing some support for the accuracy of the description of the potential energy surface away from the minimum energy path. Based on the good agreement that we obtain with the experiments (discussed below), our assumption that $H_{ij}(\mathbf{q})$ does not change significantly in going from a gas phase reactive system to a solvated system appears reasonable. Additionally, we note that it would have been possible, albeit more computationally expensive, to make every hydrogen on the cyclohexane reactive by including additional terms in the matrix of Eq. (2); however, the quality of our results suggests that this additional computational expense is not necessary for the purposes of gaining insight into the solution phase post-TS dynamics.

D. CN + cyclohexane dynamics and rare event acceleration

All of the CN + cyclohexane work described above was carried out using a locally modified version of the CHARMM software suite,[28] to which we have recently added code for carrying out reactive molecular dynamics with a generic n-state Hamiltonian matrix of the type shown in Eq. (2). Fitting was carried out using a script to interface CHARMM with the Levenberg-Marquardt algorithm implementation available within the scientific python (SciPy) library. The diagonal elements of the Hamiltonian matrix were calculated using the Merck Molecular Mechanics force-field (MMFF) in CHARMM.[29]

Both the gas phase and solution phase dynamics simulations began with NVT equilibration runs that used a leapfrog Verlet integration scheme. These were followed by subsequent NVE trajectories using a velocity verlet scheme, resulting in initial conditions that were effectively sampled using classical MD. In the gas phase, 250 stable equilibration temperature profiles were obtained with NVT runs lasting 100 ps (0.5 fs timestep) using Langevin integration with a friction coefficient of 50 ps^{-1} and a heat bath of 300 K. The subsequent NVE trajectories had a duration of 100 ps and used a 0.1 fs timestep. The 250 solution phase NVT equilibration runs lasted 200 ps (0.5 fs timestep), with a Langevin friction coefficient of 10 ps^{-1}. The subsequent NVE trajectories had a duration of 200 ps and used a 0.1 fs timestep. In the solution-phase NVT and NVE simulations, CN and C_6H_{12} were solvated within a 23.7 $Å^3$ periodic box filled with 125 molecules of CH_2Cl_2, corresponding to the experimental 298 K CH_2Cl_2 density of 1.33 g/ml.[30] Finally, we also performed simulations of energy relaxation of HCN in a periodic box of neat CH_2Cl_2 solvent with $v \sim 1$ initial excitation placed in the CH stretch. This was done via 250 solution phase NVT equilibration runs, each of which lasted 200 ps (0.5 fs timestep), with a Langevin friction coefficient of 10 ps^{-1}, and constraining the C-H distance to have a value between 1.19 and 1.24 Å using the BXD algorithm (discussed below). In the subsequent NVE trajectories, which had a duration of 200 ps and used a 0.1 fs timestep, the BXD constraint was relaxed to allow the C-H stretch to relax to equilibrium.

On the timescale of the simulations, every single gas and solution phase CN + c-C_6H_{12} trajectory was reactive, i.e., resulted in the HCN + c-C_6H_{11} radical. The algorithm we used to accelerate the probability of obtaining reactive events is called AXD,[17] which is a formally exact extension of TST, and which relies on ergodicity to accelerate reactive events through implementing phase space constraints (via velocity inversion) in a fashion that conserves angular momentum, linear momentum, and energy.[31] As such, it works equally well for both NVT and NVE simulations, and we have recently shown that it does not perturb chemical dynamics in the neighborhood of a TS so long as the distance between the phase space constraint and the TS is larger than the system's characteristic decorrelation length.[32] In the NVT simulations reported above, we implemented a phase space constraint that maintained the H–CN distance to be between 2.5 and 4.0 Å. As discussed below, this constraint is well on the reactant side of the abstraction TS. In the NVE simulations, the 2.5 Å constraint was relaxed, allowing barrier crossing and subsequent abstraction to proceed with significant acceleration, essentially by preventing diffusion of the reactants away from one another.

To obtain the potential of mean force (PMF) along the C-H stretch in both the gas-phase and the solution-phase simulations, we used the recently developed BXD (Boxed Molecular Dynamics) algorithm,[17] in conjunction with the respective NVT simulation details described above. BXD is a multiple-constraint extension of AXD (Accelerated Molecular Dynamics), which we have shown can be used to obtain accurate potentials of mean force and rate coefficients.[17,32] In the BXD simulations carried out as part of this work, we used 6 simulation boxes, with configuration space velocity inversion boundaries at 1.26 Å, 1.36 Å, 1.5 Å, 1.7 Å, 2.0 Å, 4.0 Å, and 6.0 Å. Convergence of the PMFs was monitored on each pass through the boxed configuration space. The AXD and BXD algorithms have recently been implemented in CHARMM.

E. HCN normal mode analysis

Obtaining the normal mode kinetic and potential energies of a diatomic oscillator is straightforward, since the only degree of freedom is along the internuclear axis. Calculating normal mode energies for higher dimensional systems is not

so simple, since the molecule must be appropriately aligned to determine the components of its motion and displacement that correspond to the appropriate molecular normal modes. For those reactive trajectories which yielded HCN using the methods described above, energy disposal in the nascent HCN was determined by projecting its space-fixed Cartesian velocities, $\dot{\mathbf{q}}(t)$, and coordinates, $\mathbf{q}(t)$, into the translational, rotational, and vibrational normal modes of HCN in its COM frame equilibrium geometry, $\mathbf{q}_{eq}$. In order to carry out this analysis, the nascent HCN was translated to its COM frame, and the least squares difference between the mass-weighted coordinates of the nascent HCN and those of the equilibrium HCN was minimized with respect to rigid-body rotations, using singular value decomposition – an operation which is identical to placing the rovibrationally hot HCN into the Eckart frame of the equilibrium HCN, thereby minimizing rovibrational Coriolis coupling in the reference frame of the nascent HCN.[33] Then, the projection of the Cartesian coordinates and velocities into the translational, rotational, and vibrational displacements of the equilibrium geometry was accomplished via the following relationships:[34]

$$\begin{aligned}\dot{\mathbf{Q}}(t) &= \mathbf{L}^{-1}\dot{\mathbf{q}}(t),\\ \Delta\mathbf{Q}(t) &= \mathbf{L}^{-1}\Delta\mathbf{q}(t),\end{aligned} \tag{8}$$

where $\Delta\mathbf{q}(t) = \mathbf{q}(t) - \mathbf{q}_{eq}$ is the vector of Cartesian displacements from equilibrium of a particular HCN geometry. $\Delta\mathbf{Q}(t)$ and $\dot{\mathbf{Q}}(t)$ are the respective vectors of normal mode displacements and velocities. $\mathbf{L}$ is a 3N × 3N matrix obtained from diagonalization of the mass-weighted Hessian, whose column vectors are the Cartesian displacements of the 3 translations, 2 rotations, and 3N − 5 vibrations of HCN at equilibrium. The translational and rotational eigenvectors were obtained analytically in the usual way,[35] and the vibrational eigenvectors were obtained from diagonalization of the optimized HCN Hessian. To ensure orthogonality of these vibrational eigenvectors, we utilized a Gram-Schmidt algorithm. Owing to HCN's linear geometry, the total energy partitioned into the degenerate rotational degrees of freedom and bending vibrations is cylindrically symmetric about the molecular z-axis. Thus, we report rotational energies and bending energies as respective sums of the two degenerate rotations and vibrations.

Having determined $\Delta\mathbf{Q}(t)$ and $\dot{\mathbf{Q}}(t)$, the kinetic energy of the ℓ th normal mode, $\mathbf{T}^{\ell}(t)$, was determined as

$$\mathbf{T}^{\ell}(t) = \sum_{i\alpha}\frac{m_i}{2}\left[\mathbf{L}^{\ell}_{i\alpha}\dot{\mathbf{Q}}^{\ell}(t)\right]^2, \tag{9}$$

where m is the atomic mass, i runs over the atom indices, and α runs over the Cartesian x, y, z directions. It is important to point out that in our notation, the column vectors in $\mathbf{L}$ are not the raw vectors obtained from diagonalization of the mass-weighted Hessian; rather, they have been transformed from mass-weighted to Cartesian space, and subsequently normalized using the appropriate normalization constant, N_{ℓ}. In the harmonic limit, the potential energy of the ℓ th normal mode, $\mathbf{V}^{\ell}(t)$, may be determined as

$$\mathbf{V}^{\ell}(t) = \frac{1}{2}\mu_{\ell}[\omega_{\ell}\Delta\mathbf{Q}^{\ell}(t)]^2, \tag{10}$$

where ω_{ℓ} is the frequency of the ℓ th mode, and μ_{ℓ} is the reduced mass of the mode, which is identical to N_{ℓ}^2.[36] The total energy in a particular mode, $\mathbf{E}^{\ell}(t)$, may then be calculated as

$$\mathbf{E}^{\ell}(t) = \mathbf{T}^{\ell}(t) + \mathbf{V}^{\ell}(t). \tag{11}$$

The method described above for determining total normal mode energies from the Cartesian positions and velocities is accurate in the limit of infinitesimally small displacements from the equilibrium geometry.[34,36] In the limit of large non-equilibrium displacements such as considered in this work, the accuracy of Eq. (11) falls off, primarily because Eq. (10) ignores mode-mode couplings, treating the system potential energy as separable in the normal modes. The kinetic energy, on the other hand, *is* diagonal in the normal mode displacements. The virial theorem specifies that the total energy is equipartitioned between kinetic and potential contributions, so that the average total energy over a particular time window τ, may be calculated as

$$\langle\mathbf{E}^{\ell}(t)\rangle_{\tau} \approx 2\langle\mathbf{T}^{\ell}(t)\rangle_{\tau}, \tag{12}$$

where the angled brackets indicate averages. This is the approach that we have adopted throughout this work, with all of the normal mode energies reported herein calculated using Eq. (12). So long as τ spans several vibrational periods of the ℓ th mode, then Eq. (12) may be expected to give reasonably accurate results.[34] For the (R1) reactive trajectories, energy disposal in the nascent HCN was determined by averaging for the final 60 fs of each reactive trajectory. For the (R2) trajectories, where significantly more data points were available, the averaging was carried out with $\tau = 250$ fs.

III. RESULTS AND DISCUSSION

A. Potential energy surfaces

Zero point energies for products and reactants of (R1), obtained using the UCCSD-ROHF/cc-pVDQ geometries and frequencies, as well as results from subsequent higher level single point energy calculations, are given in Table I. The zero point corrected reaction energy (–28.4 kcal mol^{-1}) obtained using the infinite basis extrapolation described in Eq. (1) is in good agreement with the experimental 298 K reaction enthalpy of –29 kcal mol^{-1},[37,38] and the corresponding

TABLE I. Zero point energies (ZPE) and single point energies of the reactants and products obtained as described in the text. All energies are in Hartrees except for the final row, which gives the difference between the product and reactant energies, and is given in units of kcal mol^{-1}.

Molecule	ZPE (UCCSD-ROHF/cc-pVDZ)	UCCSD(T) -ROHF/CBS	BB1K/6-31G*
	Reactants		
CN	0.00482	− 92.60272	− 92.64883
C_3H_8	0.10407	− 118.97403	− 119.06339
	Products		
HCN	0.01615	− 93.31448	− 93.36490
C_3H_7	0.08877	− 118.30359	− 118.39600
	E(products-reactants)		
	−2.5	− 25.9	− 30.54

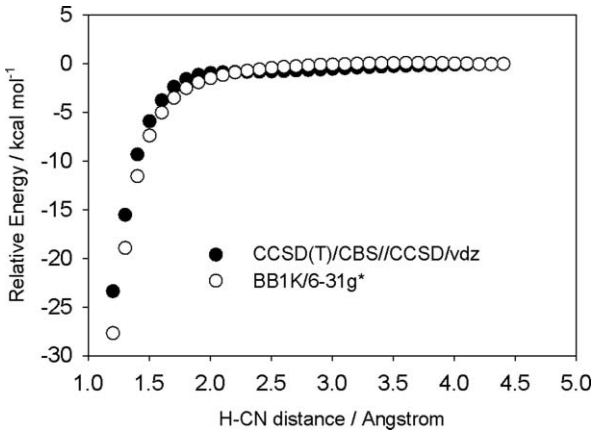

FIG. 1. Relaxed (R1) scan energies along the H–CN distance using (i) the CCSD(T)/CBS//CCSD/vdz level of theory and (ii) the reparameterized BB1K functional utilized in the direct dynamics simulations.

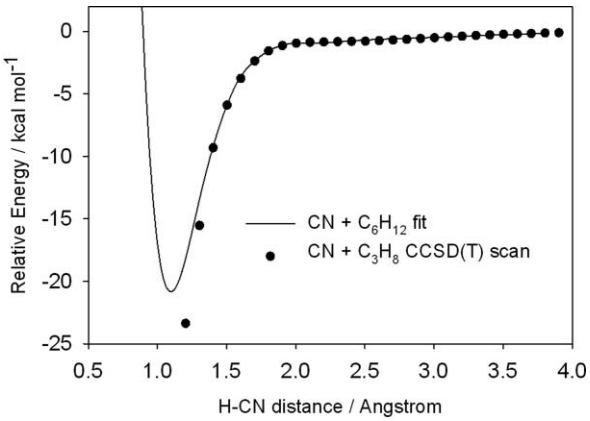

FIG. 2. Relaxed scans along the H–CN distance coordinate using (i) CCSD(T)/CBS//CCSD/vdz electronic structure theory (•) and (ii) the (R2) analytical PES (—).

energy profiles, shown in Fig. 1, are very similar to the analogous multireference results reported by Klippenstein and coworkers for CN + ethane.[39] The path shown in Fig. 1 corresponds to a barrierless abstraction for the secondary hydrogen atoms on propane, with a linear approach of the CN to the hydrogen atom, both in terms of the C–H–C and the H–CN angles. Also shown in Fig. 1 is the corresponding relaxed PES scan along the H–CN coordinate using the modified BB1K functional and the 6-31G* basis set. The BB1K/6-31G* reactant and product energies are given in Table I.

For (R2), the off-diagonal coupling elements ($H_{ij}(\mathbf{q})$ in Eq. (2)) for the analytical EVB potential energy surface, were determined by minimizing Eq. (7) using two Gaussian functions whose parameters (see Eq. (6)) were determined by fitting to the CCSD(T) energy profile for (R1) shown in Fig. 1. The energy difference between the offsets ($\varepsilon_n - \varepsilon_1$ in Eq. (2)) was fixed to –20.7 kcal mol^{-1} based on experimental data. According to the NIST thermodynamics database, the 298 K enthalpies of formation for CN and HCN are 104.00 and 31.05 kcal mol^{-1}, respectively. Combined with the experimental determination of ΔD^0_{298K} for C-H in cyclohexane (95.5 kcal mol^{-1}),[40] this gives $\Delta H^{CN+C_6H_{12}}_{298K} = -23.8$ kcal mol^{-1}. Based on cyclohexane frequency data taken from the NIST database as well as calculations by Klippenstein and coworkers carried out on the cyclohexyl radical,[41] the change in zero point energy for (R2) is ∼–3.1 kcal mol^{-1}, close to the value of –2.5 kcal mol^{-1} for (R1) given in Table I. Subtracting the change in zero point energy from the 298 K experimental reaction enthalpy gives an approximate classical reaction energy of –20.7 kcal mol^{-1}.

The parameters for the optimized Gaussians are given in Table II. The term H_{13} is still significant in the product region, however, as the zero-order reactant and product potentials have very different energies in this region, the analytical potential is almost exactly equal to the product zero-order surface. Figure 2 shows the comparison between relaxed potential energy scans along the H–CN coordinate using (i) the fitted Eq. (2) analytical PES for (R2), and (ii) relaxed CCSD(T)/CBS//CCSD/vdz PES scans for (R1). As discussed above, the reaction energy less the zero point energy for (R2) was set to be slightly less exothermic than that for (R1) determined from the CCSD(T) calculations. This can be seen clearly in Fig. 2. This does not, however, affect the quality of the fit in the early part of the reaction coordinate. Table III shows a comparison between the experimental HCN rotational constants and vibrational frequencies with those obtained at the modified BB1K/6-31G* level of theory, and using the MMFF.

TABLE II. Levenberg-Marquardt optimized parameters for the Gaussian functions making up H_{12} and H_{13} in Eq. (6).

H_{ij}	A (amplitude)	B (center)	C (width)
H_{12}	31.324	1.796	0.183
H_{13}	104.358	1.921	1.797

B. Gas phase dynamics results

1. CN + C_3H_8

A number of previous experimental and theoretical studies have examined reaction cross sections and product state distributions in the CN + H_2 → HCN + H reaction,[42] and those which examined nascent HCN product energy deposition reported excited HCN bending and CH stretching vibrations. To our knowledge, the results we report below represent the first theoretical study of product energy deposition for gas phase reactions of CN + *polyatomic* species, and represent a step toward addressing the extent to which qualitative Polanyi models are applicable to high dimensionality polyatomic systems.[43]

TABLE III. Frequencies and rotational constants of HCN obtained from experiment (NIST database), the MMFF forcefield, and the modified BB1K/6-31G* model chemistry.

	Moments of inertia (amu Å^{-2})	Frequencies (cm^{-1})
Experiment	11.404	3312, 2097, 712 (× 2)
MMFF	11.516	3470, 2019, 777 (× 2)
BB1K/6-31G*	11.131	3612, 2349, 826 (× 2)

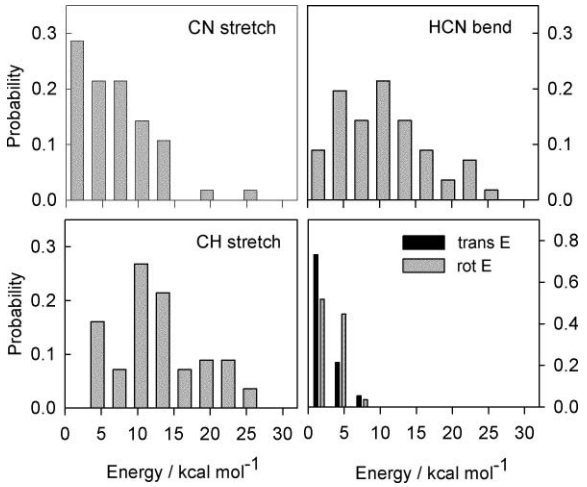

FIG. 3. Normalized distributions of energy deposited into each HCN degree of freedom for the (R1) BB1K gas phase quasiclassical direct dynamics carried out using VENUS. Results have been put in bins with a width of 3 kcal mol^{-1}.

The (R1) quasi-classical direct dynamics we report below use an impact parameter of zero, and the number of reactive trajectories is small. Consequently, the results we report below are not statistically converged. Nevertheless, the results yield significant qualitative insight. The point of these simulations was two-fold. First, the direct dynamics study of secondary H abstraction from propane by CN served as an additional reference to assess the quality of the results that we obtained using the analytical Hamiltonian for CN + cyclohexane. Second, we hoped to gain some qualitative insight into the gas phase experimental observations that the nascent HCN from various CN + RH reactions has hot C-H stretch and HCN bending modes, but thermal rotational and translational distributions.[37,44]

A total of 56 reactive trajectories (out of 74) met the energy conservation criteria discussed above. The averaged results of the QCT calculations presented in Fig. 3 show that the HCN product rotational and translational energies are very close to their thermal values at 298 K. Instead of the excess energy being deposited into HCN translational and rotational degrees of freedom, the dynamics results, shown in Fig. 3 and Table IV, clearly show that the bulk of the excess energy goes into HCN vibrational excitation, with $v \sim 0.75$ in the H-C stretch, and significant excitation ($v \sim 3.95$) in the HCN bending mode, in qualitative agreement with the experimental results. The bend excitation emerges as a particularly interesting dynamical result, especially given the fact that relaxed scans along the H–CN distance at both the CCSD-ROHF/cc-pVDZ and BB1K/6-31G* levels of theory show that the preferred HCN geometry is linear all along the reaction coordinate. As discussed in our recently published paper[14] and further in what follows, the bend excitation derives from a very soft bending potential in the region of the association transition state, and from the greater statistical likelihood of CN approach vectors with an H–CN angle that deviates from 180°. In the region of the variational transition state (i.e., the free energy maximum, whose determination is discussed further below), the distribution of HCN bend angles is peaked from 140 to 160°.

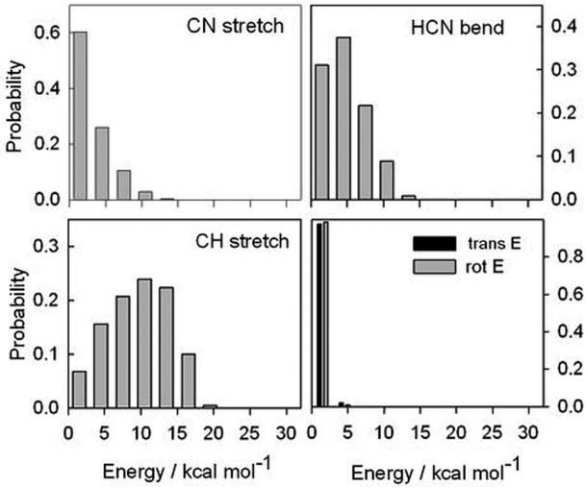

FIG. 4. Normalized distributions of energy deposited into each HCN degree of freedom for the (R2) gas phase classical dynamics carried out using the Eq. (2) analytical Hamiltonian in CHARMM. Results have been placed into bins with a width of 3 kcal mol^{-1}.

2. CN + c-C_6H_{12}

The gas phase CN + c-C_6H_{12} results obtained using the Eq. (2) analytic potential are in broad agreement with the gas phase results for (R1) discussed above. Figure 4 gives the normalized distributions of energy in each mode for the analytic MMFF classical dynamics results, and Fig. 5 shows the time dependent energy in each of the HCN vibrational degrees of freedom upon passage over the variational TS for abstraction. Both figures show that the nascent HCN has excitation in both the CH stretch and the HCN bend beyond what would be expected for a 298 K thermal distribution. According to the MMFF HCN frequencies in Table III, the harmonic energy for one quantum of vibration in the CH stretch and HCN bend modes is ~9.9 kcal mol^{-1} and ~2.2 kcal mol^{-1} respectively. As shown in Fig. 4 and Table IV, the CH stretching mode in the nascent HCN has an average energy of ~9.6 kcal mol^{-1}, and the bending mode has an average energy of

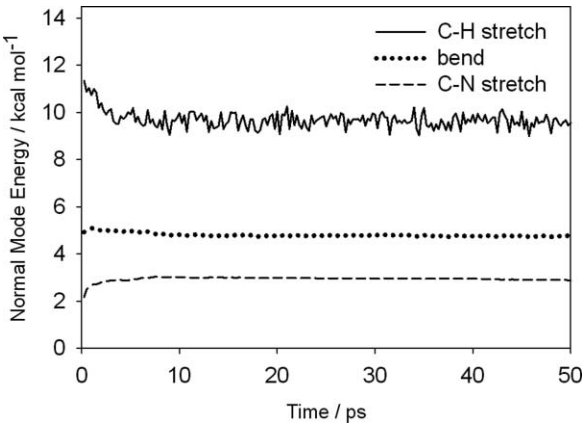

FIG. 5. Time-dependent vibrational mode energies in the nascent HCN following (R2) gas phase simulations. Zero is defined as the first passage through the HCN equilibrium CH distance. Results shown are averaged over 250 reactive trajectories. After a few picoseconds, the results are essentially time independent.

TABLE IV. Average energy disposal in nascent HCN vibrational, rotational, and translational degrees of freedom (*df*). For the quasiclassical BB1K results, which included vibrational ZPE in the initial sampling, the approximate quantum numbers (v) were obtained by subtracting the harmonic zero point energy from the average total energy, and then dividing by the energy of the appropriate BB1K harmonic vibrational frequency in Table III. For the dynamics run using Eq. (2) and the MMFF, which did not include initial vibrational ZPE, approximate quantum numbers were obtained simply through dividing by the energy of the appropriate MMFF harmonic frequency.

		$CN + C_3H_8 \rightarrow HCN + C_3H_7$ (R1) using BB1K direct dynamics		$CN + C_6H_{12} \rightarrow HCN + C_6H_{11}$ (R2) using Eq. (2) and MMFF	
df label (degeneracy)	Designation	Average energy (kcal mol^{-1})	Approximate v	Average energy (kcal mol^{-1})	Approximate v
v_1 (1)	C-N stretch	6.8	0.51	3.0	0.52
v_2 (2)	Bend	10.5	3.95	4.8	2.16
v_3 (1)	C-H stretch	12.9	0.75	9.6	0.97
Rotations (2)	N/A	3.2	...	0.6	...
Translations (3)	N/A	2.6	...	0.9	...

~4.8 kcal mol^{-1}, respectively corresponding to $v \sim 0.97$ and $v \sim 2.16$.

A direct quantitative comparison of the results in Figs. 3 and 4 is complicated by the fact that: (1) the reactive systems are different; (2) the BB1K (R1) potential gave a reaction that was ~10 kcal mol^{-1} more exothermic than the MMFF analytic potential; and (3) the (R1) initial conditions included sampling of the normal mode vibrational energies, whereas the (R2) results did not. Nevertheless, both sets of dynamics results are in good qualitative agreement. They both reproduce the experimental observations of vibrational excitation in the nascent HCN bending and CH stretching modes, without accompanying translational and rotational excitation. Furthermore, alongside Fig. 2, the results in Fig. 4 and Table IV suggest that the fitted analytic PES we developed using Eq. (6) is sufficiently accurate to providing accurate modeling of the non-equilibrium solution phase dynamics which was a primary aim of this study.

C. Solution phase dynamics results

Figure 6 shows the relative PMF for (R2) along the H–CN abstraction coordinate in both the gas-phase and solution-phase dynamics simulations, obtained using the BXD method. Despite the fact that the reaction is a barrierless process on the potential energy surface, both the gas-phase and solution-phase simulations show maxima in their respective PMFs. These maxima occur at very similar values of the reaction coordinate (~1.9 Å and 1.95 Å), and we have set the zero of both PMFs at this point. The origin of this maximum is primarily entropic,[45] corresponding to a reduction in relative fragment rotational and translational degrees of freedom as CN approaches c-C_6H_{12} to abstract a hydrogen atom. The potential of mean force in the reactant region is somewhat different in the gas phase and in solution, suggesting at first sight a significant difference in the rate constants for the two reactions. However, experiments show that the rate constants are in fact very similar. The solution phase data[14] can be analyzed to provide a room temperature rate constant of ~8.4 × 10^{-10} cm^3 molecule^{-1} s^{-1} for the CN + c-C_6H_{12} reaction. The rate constant at room temperature for the gas phase CN + c-C_6H_{12} reaction has been measured as ~2.7 × 10^{-10} cm^3 molecule^{-1} s^{-1}.[40] It is known[46] that relative free energies for bimolecular and association reactions cannot be obtained simply from inspection of numerically derived PMFs. In particular, the PMFs shown in Fig. 6 are not fully converged with respect to sampling of all relative rotational orientations of the two reactants at large H–CN distances, and this may contribute to the apparent difference between the two curves in the reactant region. For the primary aim of this article, however, these differences are not significant, because the PMFs in the transition state and post-transition state regions are nearly identical, and it is these that determine the product energy partitioning.

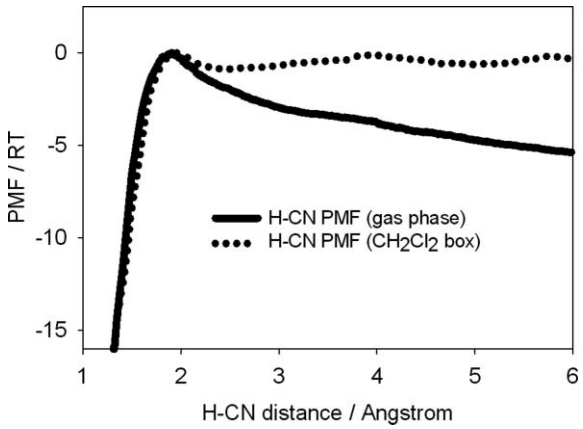

FIG. 6. Plot of the PMF along the H–CN abstraction coordinate for (R2) in the gas phase and solvated in a CH_2Cl_2 box

Figure 7 depicts overlays taken from NVE simulations of the CN + c-C_6H_{12} geometries at the moment of passage over the gas phase and solution phase free energy maxima, and shows that the range of geometries sampled in the gas and solution phases is largely similar. Taken together, Figs. 6 and 7 suggest that the gross features of the dynamics en route to products following TS passage should be substantially similar in solution and in the gas phase.

Figure 8 shows normalized distributions of the energy deposition into the HCN degrees of freedom within the first picosecond following passage over the solution phase variational TS shown in Fig. 6. The distributions are similar to the corresponding CN + c-C_6H_{12} gas phase distributions shown in Fig. 4, consistent with the state specific vibrational excitation reported from our experimental studies,[14] which

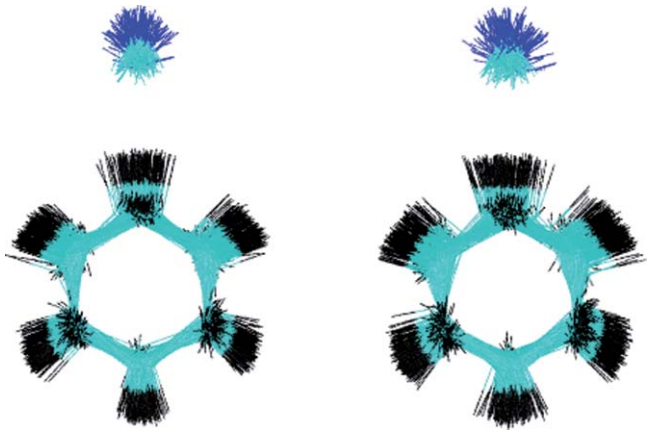

FIG. 7. Superpositions of the ensemble of CN + c-C_6H_{12} geometries at the point where they pass over their gas and solution phase free energy barriers. The left and right hand structures, respectively, correspond to the gas and solution phases. Their similarity explains in part why, at short times, the gas phase reaction specificity is similar to that in solution phase. The figures also shed light on the origin of the bend excitation, since the relative orientation of the CN with respect to c-C_6H_{12} carves out a large range of H–CN angles.

show that HCN forms preferentially with $v = 1$ in the CH stretch and HCN bend excitation up to $v = 2$. Comparison of Figs. 4 and 8 points to at least a weak solvent effect on the HCN product energy distributions. The Fig. 8 solution phase CH stretch distribution peaks at ∼7 kcal mol^{-1}, compared to a peak in the Fig. 4 gas phase distribution at ∼10–12 kcal mol^{-1}.

While the short-time vibrational energy deposition is essentially identical in both gas and solution phase owing to similarities in the post-TS free energy profile in Fig. 6, the same is not true for the time-dependent mode energies, which are shown in Fig. 9 for the nascent HCN in the solution phase simulations (and Fig. 5 for the gas-phase calculations). In both Figs. 5 and 9, the zero is defined at the time of first passage through the HCN equilibrium CH distance. Figure 9 clearly shows again that the average energy in each normal mode of

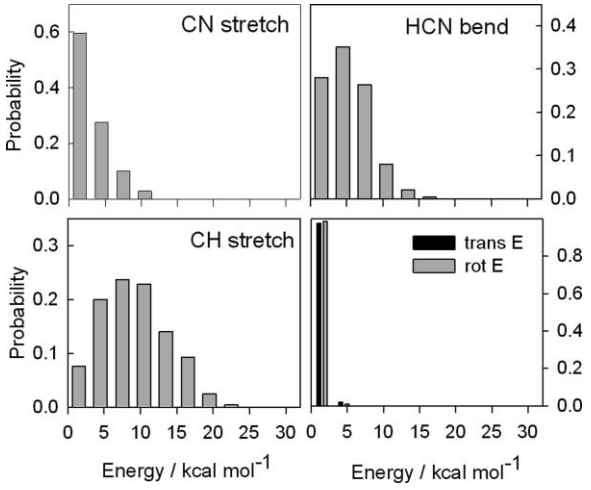

FIG. 8. Normalized distributions of energy deposited into each HCN degree of freedom for the (R2) solution phase classical dynamics carried out using Eq. (2) analytical Hamiltonian in CHARMM. Results have been placed into bins with a width of 3 kcal mol^{-1}

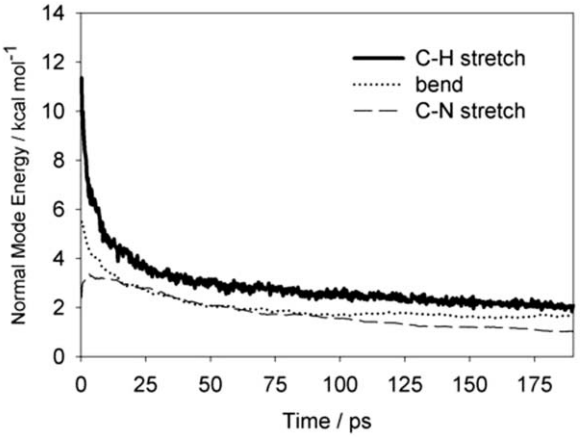

FIG. 9. Time-dependent vibrational mode energies in the nascent HCN following abstraction of a hydrogen atom from c-C_6H_{12} in the solution phase simulations. Results shown are averaged over 250 reactive trajectories.

the nascent HCN is similar to that in the corresponding gas phase reaction at very short times. At longer times, however, energy is dissipated to the solvent degrees of freedom. One of the most unexpected features of the data shown in Fig. 9 is the fact that the energy decay profiles in each mode show distinct timescales – a fast decay at short times, and a slower decay at long times.

A comparison of the results obtained for HCN relaxation following from $v \sim 1$ CH stretch excitation in neat solvent versus CH stretch relaxation in HCN following (R2) in the same solvent is shown in Fig. 10. To a good approximation, the decay of CH excitation averaged over the ensemble of trajectories in the free CH_2Cl_2 solvent follows an exponential decay, which has been pointed out in other studies:[13]

$$\frac{\langle E_v(t)\rangle - \langle E_v(\infty)\rangle}{\langle E_v(0)\rangle - \langle E_v(\infty)\rangle} = \exp(-t/\tau), \tag{13}$$

where $\langle E_v(t)\rangle$ is the average energy at time t in mode v (here the CH stretch), $\langle E_\infty(t)\rangle$ is the average equilibrium energy in mode v (taken to be kT based on the equipartition principle),

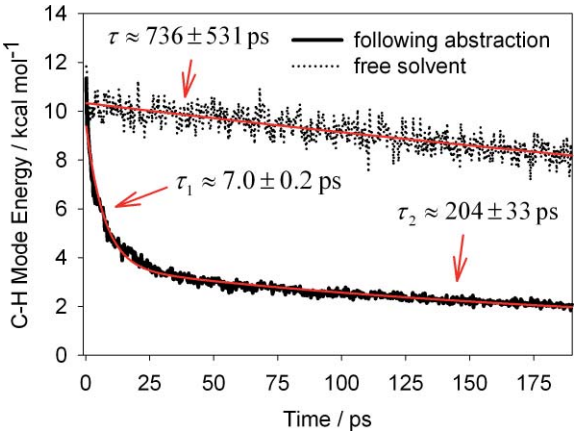

FIG. 10. Comparison of the relaxation of the CH stretch mode energy in HCN (1) following abstraction of a hydrogen atom from C_6H_{12} in CH_2Cl_2 solvent, and (2) following $v \sim 1$ excitation of the CH stretch mode in free CH_2Cl_2 solvent. For each curve, the results shown are averaged over 250 trajectories.

and $\langle E_v(0)\rangle$ is the average energy at $t = 0$. Using Eq. (13), the decay of CH energy for HCN in a periodic box of neat CH_2Cl_2 gives a value of $\tau \sim 736 \pm 531$ ps. The CH energy profile in Figs. 9 and 10 was fit with a biexponential decay analogous to Eq. (12), i.e.,

$$\frac{\langle E_v(t)\rangle - \langle E_v(\infty)\rangle}{\langle E_v(0)\rangle - \langle E_v(\infty)\rangle} = A\exp(-t/\tau_1) + B\exp(-t/\tau_2), \quad (14)$$

where τ_1 and τ_2 are the respective time constants for decay at short times and long times, and A and B are constrained so that they sum to unity. Using Eq. (14), the fitted value of the time constant for long-time decay for the CH stretch mode, τ_2, has a value of $\sim 204 \pm 33$ ps, in close agreement with the experimental decay time constants of 144 ± 8 ps obtained from IR pump-probe experiments carried out on HCN in CH_2Cl_2 and ~ 1.0 M C_6H_{12}.[14] Comparison of the long-time predictions of our dynamics simulations, after HCN and C_6H_{11} have undergone significant diffusion, suggest that the conditions for the experimental pump-probe measurements give rise to HCN energy transfer efficiencies larger than what would be expected in neat CH_2Cl_2. The time constant for short-time decay, τ_1, has a value of $\sim 7 \pm 0.2$ ps, more than an order of magnitude faster than τ_2.

The observation of multiexponential vibrational energy decay in the product HCN after reaction in solution is intriguing. In the gas phase, intramolecular vibrational energy redistribution (IVR) can follow a complicated time course. In the present case, the gas phase and solution results suggest that the HCN product does not display significant IVR on the timescales considered here. The difference in the HCN energy relaxation profiles shown in Fig. 10 arises because of time dependent energy relaxation efficiencies for HCN as it diffuses away from its *c*-C_6H_{11} co-product into the bulk CH_2Cl_2 solvent. At short times, energy relaxation of the nascent HCN is extremely efficient given its proximity to *c*-C_6H_{11}, which serves as an efficient acceptor of the vibrational energy in the nascent HCN, and also facilitates fast energy transfer to the solvent. As the HCN and *c*-C_6H_{11} diffuse away from one another through the CH_2Cl_2 solvent matrix, HCN energy relaxation to the solvent bath becomes less efficient, more closely resembling the relaxation decay profiles for isolated HCN in CH_2Cl_2. This explanation is qualitatively compatible with Fermi's Golden Rule – with the caveat that the density of accepting states for the HCN vibrational energy is effectively time dependent. A detailed analysis of these effects is beyond the scope of the present paper, but a combined theoretical and experimental analysis will be presented in a subsequent publication.[47]

IV. CONCLUSIONS

In this work, we report the first theoretical studies of post-transition state dynamics for H atom abstractions of CN + polyatomic species. Using high-level electronic structure theory, a reparameterized density functional, a newly developed analytic reactive PES, and a recently implemented rare-event acceleration algorithm, we carried out both quasi-classical and classical non-equilibrium molecular dynamics simulations to investigate the reaction of CN with propane and cyclohexane in the gas phase and in a CH_2Cl_2 solvent. The results suggest that the solvent perturbations to the reactive free energy surface are small. This leads to very similar post-reaction product energy partitioning in both the gas and the solvent. In both sets of simulations, the nascent HCN is formed with vibrational excitation in both its CH stretching and HCN bending coordinates. The similarity in the energy deposition arises in part because of the similarity in the distributions of molecular geometries at the respective gas and solution phase variational association transition states, suggesting the utility of Polanyi type rules in qualitatively rationalizing the early time dynamical outcomes of solution phase bimolecular reactions for polyatomic species. This study highlights the fact that non-equilibrium energy distributions following solution phase bimolecular reactions may persist for hundreds of picoseconds, despite frictional damping. In addition to the reactive solution phase dynamics, we also carried out non-equilibrium MD simulations for HCN in CH_2Cl_2, and show that the HCN energy decay profile shows notable differences compared to HCN which is formed from a chemical reaction. We note that all the dynamics calculations performed in this work use either classical or quasi-classical trajectory propagation. The good agreement with experiment for the observed degree of vibrational excitation in the nascent products, and for the rate of decay by coupling to solvent, suggest that this classical approach captures the essential physics of vibrational energy transfer very well.[12,13,48]

Within the molecular modeling community, the most widely used approaches for studying condensed phase chemical kinetics utilize thermostatted equilibrium MD, canonical rate theory, and Monte-Carlo Sampling. The implicit assumption with all of these approaches is that the timescales on which chemical reactions occur are much slower than (and consequently decoupled from) thermalization timescales. The present study shows that energy transfer in the post-transition state region is in fact relatively slow, and, by microscopic reversibility, this must be true in the pre-transition state region for reactions similar to the reverse of that studied here. For the present system, none of the modeling suggests that the rate of the elementary chemical reaction being studied would deviate from that predicted by a statistical rate theory. However, non-thermal energy distributions as formed in the post-transition state region might lead to breakdown of statistical theory for a hypothetical subsequent step. In this context, further theoretical and experimental studies will help unravel the extent to which such non-equilibrium dynamical effects are significant in other condensed phase chemical reactions of the sorts encountered in, e.g., biochemistry and synthetic chemistry.

ACKNOWLEDGMENTS

We thank David Tew for helpful conversations in setting up the normal mode projection algorithm, and Robert Best for exchanges that facilitated development of the CHARMM code to perform the calculations described herein. Funding for D.R.G., A.J.O.E., and J.N.H. was provided by EPSRC Programme Grant No. EP/G00224X/1. A.J.O.E. gratefully ac-

knowledges the Royal Society and Wolfson Foundation for a Research Merit Award.

[1]G. A. Voth and R. M. Hochstrasser, J. Phys. Chem. **100**, 13034 (1996).
[2]J. C. Owrutsky, D. Raftery, and R. M. Hochstrasser, Annu. Rev. Phys. Chem. **45**, 519 (1994).
[3]C. G. Elles and F. F. Crim, Annu. Rev. Phys. Chem. **57**, 273 (2006).
[4]I. Benjamin, J. Chem. Phys. **103**, 2459 (1995).
[5]K. Bolton, W. L. Hase, and C. Doubleday, J. Phys. Chem. B **103**, 3691 (1999); J. M. Anna and K. J. Kubarych, J. Chem. Phys. **133**, 174506 (2010).
[6]G. Gershinsky and B. J. Berne, J. Chem. Phys. **110**, 1053 (1999).
[7]D. Raftery, M. Iannone, C. M. Phillips, and R. M. Hochstrasser, Chem. Phys. Lett. **201**, 513 (1993).
[8]U. Lourderaj, K. Park, and W. L. Hase, Int. Rev. Phys. Chem. **27**, 361 (2008); L. P. Sun, K. Y. Song, and W. L. Hase, Science **296**, 875 (2002).
[9]Y. Oyola and D. A. Singleton, J. Am. Chem. Soc. **131**, 3130 (2009).
[10]D. R. Glowacki, C. H. Liang, S. P. Marsden, J. N. Harvey, and M. J. Pilling, J. Am. Chem. Soc. **132**, 13621 (2010).
[11]J. L. Skinner and P. G. Wolynes, J. Chem. Phys. **69**, 2143 (1978); J. L. Skinner, Theor. Chem. Acc. **128**, 147; E. A. Carter, G. Ciccotti, J. T. Hynes, and R. Kapral, Chem. Phys. Lett. **156**, 472 (1989); A. C. Moskun, A. E. Jailaubekov, S. E. Bradforth, G. H. Tao, and R. M. Stratt, Science **311**, 1907 (2006); I. Benjamin, J. Chem. Phys. **129**, 11 (2008); N. Winter, I. Chorny, J. Vieceli, and I. Benjamin, *ibid.* **119**, 2127 (2003).
[12]S. G. Ramesh and E. L. Sibert, J. Chem. Phys. **125**, 244512 (2006); *ibid.* **125**, 244513 (2006); *ibid.* **124**, 234501 (2006).
[13]R. M. Whitnell, K. R. Wilson, and J. T. Hynes, J. Phys. Chem. **94**, 8625 (1990); J. Chem. Phys. **96**, 5354 (1992).
[14]S. J. Greaves, R. A. Rose, T. A. A. Oliver, D. R. Glowacki, M. N. R. Ashfold, J. N. Harvey, I. P. Clark, G. M. Greetham, A. W. Parker, M. Towrie, and A. J. Orr-Ewing, Science **331**, 1423 (2011).
[15]D. Raftery, E. Gooding, A. Romanovsky, and R. M. Hochstrasser, J. Chem. Phys. **101**, 8572 (1994).
[16]A. C. Crowther, S. L. Carrier, T. J. Preston, and F. F. Crim, J. Phys. Chem. A **113**, 3758 (2009).
[17]D. R. Glowacki, E. Paci, and D. V. Shalashilin, J. Phys. Chem. B **113**, 16603 (2009).
[18]D. Feller and D. A. Dixon, J. Chem. Phys. **115**, 3484 (2001); J. M. L. Martin, Chem. Phys. Lett. **259**, 669 (1996).
[19]M. J. Frisch, G. W. Trucks, H. B. Schlegel, G. E. Scuseria, M. A. Robb, *et al.*, GAUSSIAN *03* (Gaussian, Inc., Pittsburgh, 2003); H.-J. Werner, P. J. Knowles, R. Lindh, F. R. Manby, M. Schültz, *et al.*, MOLPRO, version 2006.1, a package of *ab initio* programs, see www.molpro.net
[20]X. C. Hu, W. L. Hase, and T. Pirraglia, J. Comput. Chem. **12**, 1014 (1991); W. L. Hase, R. J. Duchovic, X. Hu, A. Komornicki, K. F. Lim, D.-h. Lu, G. H. Peslherbe, K. N. Swamy, S. R. V. Linde, A. Varandas, H. Wang, and R. J. Wolf, QCPE Bull. **16**, 671 (1996).
[21]W. L. Hase and D. G. Buckowski, Chem. Phys. Lett. **74**, 284 (1980).
[22]R. N. Porter and M. Karplus, J. Chem. Phys. **40**, 1105 (1964); M. G. Evans and M. Polanyi, Trans. Faraday Soc. **34**, 0011 (1938); M. G. Evans and E. Warhurst, Trans. Faraday Soc. **34**, 0614 (1938); G. G. Balint-Kurti, Adv. Chem. Phys. **30**, 137 (1975).
[23]P. Lancaster, Numer. Math. **6**, 377 (1964).
[24]S. C. L. Kamerlin and A. Warshel, Faraday Discuss. **145**, 71 (2010); A. Warshel and R. M. Weiss, J. Am. Chem. Soc. **102**, 6218 (1980).
[25]Y. T. Chang and W. H. Miller, J. Phys. Chem. **94**, 5884 (1990).
[26]Y. Kim, J. C. Corchado, J. Villa, J. Xing, and D. G. Truhlar, J. Chem. Phys. **112**, 2718 (2000).
[27]K. F. Wong, J. L. Sonnenberg, F. Paesani, T. Yamamoto, J. Vanicek, W. Zhang, H. B. Schlegel, D. A. Case, T. E. Cheatham, W. H. Miller, and G. A. Voth, J. Chem. Theory Comput. **6**, 2566 (2010).
[28]B. R. Brooks, C. L. Brooks III, A. D. Mackerell, Jr., L. Nilsson, R. J. Petrella, B. Roux, Y. Won, G. Archontis, C. Bartels, S. Boresch, A. Caflisch, L. Caves, Q. Cui, A. R. Dinner, M. Feig, S. Fischer, J. Gao, M. Hodoscek, W. Im, K. Kuczera, T. Lazaridis, J. Ma, V. Ovchinnikov, E. Paci, R. W. Pastor, C. B. Post, J. Z. Pu, M. Schaefer, B. Tidor, R. M. Venable, H. L. Woodcock, X. Wu, W. Yang, D. M. York, and M. Karplus, J. Comput. Chem. **30**, 1545 (2009).
[29]T. A. Halgren, J. Comput. Chem. **17**, 490 (1996).
[30]L. X. Dang, J. Chem. Phys. **110**, 10113 (1999).
[31]E. Martinez-Nunez and D. V. Shalashilin, J. Chem. Theory Comput. **2**, 912 (2006); D. V. Shalashilin and D. L. Thompson, ACS Symp. Ser. **678**, 81 (1997) (Highly Excited Molecules); J. Chem. Phys. **107**, 6204 (1997); J. Phys. Chem. A **101**, 961 (1997).
[32]D. R. Glowacki, E. Paci, and D. V. Shalashilin, J. Chem. Theory Comput. **7**, 1244 (2011).
[33]K. N. Kudin and A. Y. Dymarsky, J. Chem. Phys. **122**, 2 (2005); G. R. Kneller, J. Chem. Phys. **128**, 6 (2008); E. A. Coutsias, C. Seok, and K. A. Dill, J. Comput. Chem. **26**, 1663 (2005); J. H. Challis, J. Biomech. **28**, 733 (1995).
[34]L. M. Raff, J. Chem. Phys. **89**, 5680 (1988).
[35]W. H. Miller, N. C. Handy, and J. E. Adams, J. Chem. Phys. **72**, 99 (1980).
[36]J. C. Corchado and J. Espinosa-Garcia, Phys. Chem. Chem. Phys. **11**, 10157 (2009).
[37]W. P. Hess, J. L. Durant, and F. P. Tully, J. Phys. Chem. **93**, 6402 (1989); A. G. Maki and R. L. Sams, J. Chem. Phys. **75**, 4178 (1981).
[38]D. F. McMillen and D. M. Golden, Annu. Rev. Phys. Chem. **33**, 493 (1982).
[39]Y. Georgievskii and S. J. Klippenstein, J. Phys. Chem. A **111**, 3802 (2007).
[40]T. Yu, D. L. Yang, and M. C. Lin, Chem. Phys. **162**, 449 (1992).
[41]A. M. Knepp, G. Meloni, L. E. Jusinski, C. A. Taatjes, C. Cavallotti, and S. J. Klippenstein, Phys. Chem. Chem. Phys. **9**, 4315 (2007).
[42]U. Manthe and F. Matzkies, Chem. Phys. Lett. **282**, 442 (1998); W. Zhu, J. Z. H. Zhang, Y. C. Zhang, Y. B. Zhang, L. X. Zhan, S. L. Zhang, and D. H. Zhang, J. Chem. Phys. **108**, 3509 (1998); G. A. Bethardy, A. F. Wagner, G. C. Schatz, and M. A. terHorst, *ibid.* **106**, 6001 (1997); C. Coletti and G. D. Billing, *ibid.* **113**, 11101 (2000); G. A. Bethardy, F. J. Northrup, G. He, I. Tokue, and R. G. Macdonald, *ibid.* **109**, 4224 (1998); T. Takayanagi, M. A. terHorst, and G. C. Schatz, *ibid.* **105**, 2309 (1996); M. A. terHorst, G. C. Schatz, and L. B. Harding, *ibid.* **105**, 558 (1996).
[43]J. B. Liu, K. Y. Song, W. L. Hase, and S. L. Anderson, J. Am. Chem. Soc. **126**, 8602 (2004).
[44]G. A. Bethardy, F. J. Northrup, and R. G. Macdonald, J. Chem. Phys. **105**, 4533 (1996); **102**(20), 7966 (1995); L. R. Copeland, F. Mohammad, M. Zahedi, D. H. Volman, and W. M. Jackson, *ibid.* **96**, 5817 (1992); V. R. Morris, F. Mohammad, L. Valdry, and W. M. Jackson, Chem. Phys. Lett. **220**, 448 (1994).
[45]A. Fernandez-Ramos, J. A. Miller, S. J. Klippenstein, and D. G. Truhlar, Chem. Rev. **106**, 4518 (2006).
[46]M. K. Gilson, J. A. Given, B. L. Bush, and J. A. McCammon, Biophys. J. **72**, 1047 (1997); S. Doudou, N. A. Burton, and R. H. Henchman, J. Chem. Theory Comput. **5**, 909 (2009).
[47]D. R. Glowacki, R. A. Rose, S. J. Greaves, A. J. Orr-Ewing, and J. N. Harvey, "Mapping energy flow dynamics in the wake of solution phase bimolecular reactions," Nat. Chem. (submitted).
[48]J. S. Bader and B. J. Berne, J. Chem. Phys. **100**, 8359 (1994).